

DEFECT-CREATION MECHANISMS IN HIGH-ENERGY ELECTRON IRRADIATED A-Si:H SOLAR CELLS

A. Klaver, J. W. Metselaar, M. Zeman, R. A. C. M. M. van Swaaij
Delft University of Technology, DIMES - ECTM, P. O. Box 5053, NL-2600 GB Delft, The Netherlands

Abstract— For an extensive use of a-Si:H solar cells in a space environment, it is important to be able to predict their End-of-Life (EOL) efficiency for a given mission due to irradiation. However, in the literature the defect creation mechanism of high-energy charged particle irradiation of a-Si:H solar cells is still debated. We present an alternative method to deduct the defect creation mechanism by irradiating a-Si:H solar cells with varying i-layer thickness and then matched the results to computer simulations. Our main point of interest is obtaining the defect creation depth profile. Different profiles, corresponding to different defect creation mechanisms are tested. Two other assumptions in the model are also investigated: The influence of the dark activation energy of the doped layers on the V_{oc} degradation, and the difference of profiling the defect creation depth profile using total recombination or the recombination on weak bonds.

Keywords— a-Si:H solar cells, degradation, modeling.

I. INTRODUCTION

In space, solar cells are subjected to a harsh environment. One of the more important damage mechanisms for crystalline silicon (c-Si) and gallium arsenide (GaAs) solar cells is the high-energy charged-particle irradiation. Hydrogenated amorphous silicon (a-Si:H) solar cells have great potential for space applications, because they can be produced inexpensively, are lightweight, and are radiation hard. If these cells are going to be used in space, it is important to be able to predict their End-of-Life (EOL) efficiency for a given mission. Computer simulations can be a valuable aid to obtain accurate EOL predictions. However, in order to develop a computer model to describe the effects of the irradiation on the cell performance, quantitative and qualitative information

about the degradation mechanisms inside the solar cells are required. A typical method to obtain an indication for the EOL performance in a space environment is to irradiate the cells with a 1-MeV electron beam [1].

In this contribution we discuss various defect creation mechanisms as proposed in literature corresponding to this irradiation and we present a model to calculate the changes in performance of the solar cell after 1-MeV electron irradiation based on the changes in the individual layers of the solar cell. In the model different defect creation depth profiles (DCDP) are considered which are linked to different defect creation processes.

In order to validate the model and to extract the DCDP, we have matched measurement and simulation results of the change in Quantum Efficiency (QE) and the external parameters of a-Si:H solar cells with varying intrinsic layer thickness (150 nm – 900 nm) following 1-MeV electron-beam irradiation. We will show that recombination through the band tail states gives the best match between simulations and measurement results.

II. DEFECT MECHANISMS

A. General information

When a charged high-energy particle (electrons and/or protons) moves through a material, it interacts with this material in a number of ways. Most energy of the incident particle is dissipated through ionization processes. For instance, high-energy electrons transfer kinetic energy through Coulomb interaction to the electrons in the material and electron-hole (e-h) pairs are generated. The amount of energy dissipated through these processes is dependent on the energy, type of particle and material, and is determined by the Ionizing Energy Loss (IEL). This quantity is given in MeVcm^2/g . The average (kinetic) energy, E , needed to generate one electron-hole pair is dependent on the bandgap, E_g , of

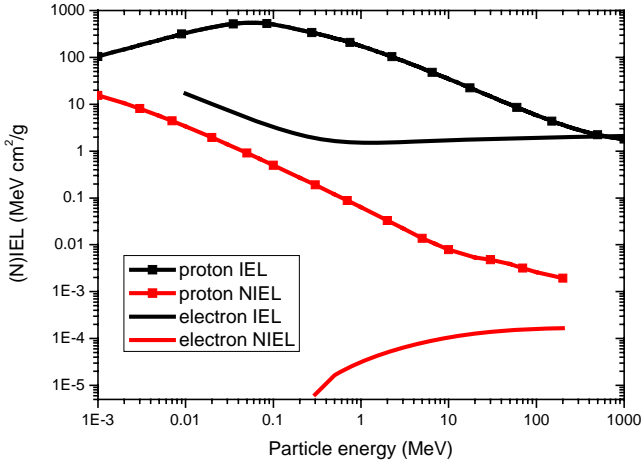


Figure 1: IEL and NIEL values for proton and electron irradiation for various particle energies.

the material and is given by:

$$E = 2.73 \cdot E_g + 0.5 \text{ [eV]} \quad (1)$$

This relation was found to be applicable to a large number of materials [2].

A fraction of the incident particle energy is, however, dissipated through so-called non-ionizing processes (Non-Ionizing Energy Loss, NIEL). Here, kinetic energy is transferred from the particle to the nuclei in the material. With this process interstitials can be created and Si-Si or Si-H bonds in the material can be broken. Si-H bonds are broken more easily, because the maximum energy transfer of a 1-MeV electron is 2100 eV for a collision with an H-atom and only 74 eV for a Si-atom.

With high-energy electron irradiation there is a third energy loss process, so-called Bremsstrahlung. When an energetic electron moves through a material with heavy atoms, high energetic x-rays are generated. However, most x-rays generated in the cell will not be absorbed in the cell to contribute to the degradation. Therefore, we will not consider this process further in this article.

Figure 1 shows the NIEL and IEL values for proton and electron irradiation for c-Si as a function of the kinetic energy of the incident particle. For the calculations of the NIEL values a displacement threshold value of 21 eV is used. For the proton and electron IEL the so-called electronic and collision stopping power are given, respectively [3-4].

For low-energy electrons, below 0.2 MeV, the only important energy loss mechanism is through ionization processes. The IEL for electron irradiation shows a minimum at 0.5 MeV. For higher kinetic energies both

the IEL and NIEL are increased. The ratio between IEL and NIEL, however, is decreased. The IEL for proton irradiation shows a maximum at 0.1 MeV. For protons, due to their higher mass, the ratio between IEL and NIEL is lower, compared to the ratio for electrons, i.e., a higher fraction of the energy is dissipated through the generation of displacements in the material with proton irradiation. For a-Si:H the values are expected to be very similar, because the IEL and NIEL are mainly dependent on the density of the material and the type of atoms, and not on the electrical properties of the material.

B. Literature review

It is still under debate which defect mechanism is important for the degradation of solar cells following irradiation. Some groups have studied the degradation and tried to explain the defect creation mechanisms resulting from high-energy charged-particle irradiation. We will now review the most important findings reported in literature.

Lord *et al.* [5] reported the effects of 40-keV electron and 1-MeV proton irradiation on single and triple junction a-Si:H solar cells, by characterizing the cells by the light and dark J - V curves. They assume that the defects are generated uniformly across the solar cells and show, using simulations that these defects have energy levels close to mid bandgap. This increase in defect density leads to a lowering of the electric field across the solar cell and to a drop in the current collection. Vendura *et al.* [6] studied triple junction solar cells after 1-MeV proton irradiation and claimed that the degradation of a-Si:H cells is due to displacement processes based on expected similarities with c-Si solar cells.

Srouf *et al.* [7] investigated the solar cell degradation using different energies and types of irradiation (electron, proton and x-ray). They conclude that degradation by charged high-energy particles is dominated by ionizing processes (IEL) and not by displacement processes (NIEL). They assume that the ionization-produced charge is trapped at pre-existing centers at a rate directly proportional to the ionizing dose. This trapped charge leads to a reduction of the electric field and the current collection. However, Walters *et al.* [8] could not find a good correlation between the ionizing dose and the degradation of a-Si:H triple junction cells following electron beam irradiation using 3 different energies and fluence.

Danesh *et al.* [9] presented the degradation of the opto-electronic and structural properties of a-Si:H following 18-MeV electron irradiation and suggest that radiation induced degradation is similar to the Staebler-

Wronski effect [10], i.e., the recombination of the charge carriers increases the defect density in the material following irradiation [11]. Kishimoto *et al.* [12] measured the radiation-induced current and photocurrent of a 17-MeV proton degraded a-Si:H. They conclude that proton irradiation is to a large extent similar to the Staebler-Wronski effect, although some differences are noted as well. In addition, it is claimed that the collisional displacement processes in the material are accommodated by local atomic relaxation, because of the high structural flexibility of a-Si:H. Time Resolved Microwave Conductivity (TRMC) results on the degradation of a-Si:H samples using a 3-MeV electron-beam by Klaver *et al.* [13] suggested the same. Diehl *et al.* [14] came to the same conclusion after studying a-Si:H films with Constant Photocurrent Method (CPM) following 20-keV irradiation.

C. Alternative procedure to determine defect creation mechanism

In this paper we present an alternative method to investigate the defect creation mechanism. We try to do this by determining the defect creation depth profile (DCDP) due to the high-energy electron irradiation assuming different defect creation processes (like displacement, ionization, and recombination processes). To determine this DCDP, solar cells with varying i-layer thickness are irradiated with a 1-MeV electron beam. By carefully matching computer simulations of the J - V characteristics and QE with experimental results, the DCDP for each solar cell can be determined.

If the defect creation mechanism is correlated to displacement damage or direct ionization processes, the DCDPs are expected to be constant throughout the solar cell and equal for each solar cell thickness irradiated with the same fluence and particle, because the energy of the electron beam is dissipated uniformly throughout the whole solar cell.

If the defect creation mechanism is linked to recombination processes, the DCDP is similar in shape to the recombination profile under the irradiation. In case of 1-MeV electron irradiation of p-i-n a-Si:H solar cells, the recombination density is higher in the bulk and the near i-n interface as compared to the p-i interface and thus in this case the defects would be created mainly in the bulk and back of the cell. In addition, in thin solar cells the recombination rate density in the i-layer is significantly lower as compared to thicker cells due to the higher electrical field across the thinner cell, which will increase the charge-carrier collection. As a result,

the defect density is more increased in the thicker solar cells as compared to thin cells.

III. MODEL DESCRIPTION

A. The ASA device simulator

The degradation model presented in this paper to calculate the EOL performance of solar cells subjected to 1-MeV electrons is build around the device simulator ‘Advanced Semiconductor Analysis’ (ASA), which has been developed at the Delft University of Technology [15]. This program is a two-terminal, steady-state device simulator in which various models for describing the a-Si:H defect density of states (DOS) are included and in which appropriate recombination-generation statistics are used. It is based on the adapted drift-diffusion model with the free electron and hole concentration as well as the electrostatic potential as variables, and uses the Poisson equation and the two continuity equations for electrons and holes.

ASA is used to simulate the quantum efficiency and the external parameters of the solar cells given all the electrical and optical properties of all layers in the cell. It has been successfully applied to study as-deposited a-Si:H [16], microcrystalline [17], tandem [18] and transverse solar cells [19], as well as light-degraded a-Si:H cells [20].

B. Baseline set

The DOS of the as-deposited a-Si:H solar cells are modeled in the following way: The valence and conduction band are described using the effective state density approach. Exponential valence and conduction bands tails are assumed. To calculate the as-deposited defect-density-of-states profile in the solar cell the defect-pool model [21] is used. In this model the defect DOS is dependent on the local weak-bond density and the Fermi-level. According to the defect-pool model three defect states can be identified: D_h defect states (positively charged defects), D_z defect states (neutral defects), and D_e defect states (negatively charged defects). Shockley-Read-Hall recombination statistics is approximated by the Taylor-Simmons model. Important ASA input parameters corresponding to the as-deposited state are given in Table I. Using this parameter set, ASA provides a good match with the experimental performance characteristics of the as-deposited solar cells.

Doped layers	
Activation energy p-layer	0.55 eV
Activation energy n-layer	0.35 eV
Intrinsic layer	
Mobility gap	1.79 eV
Effective DOS valence band	$4 \times 10^{26} \text{ m}^{-3}$
Effective DOS conduction band	$6 \times 10^{26} \text{ m}^{-3}$
DOS at valence band edge	$1 \times 10^{27} \text{ m}^{-3} \text{ eV}^{-1}$
Characteristic energy valence band tail	0.05 eV
Hydrogen concentration	$5 \times 10^{27} \text{ m}^{-3}$
Si-Si bond concentration	$2 \times 10^{29} \text{ m}^{-3}$
Width of defect pool	0.175 eV
Position of defect pool (relative to valence band)	1.17 eV
Electron mobility	$15 \times 10^{-4} \text{ m}^2 \text{ V}^{-1} \text{ s}^{-1}$
Hole mobility	$2 \times 10^{-4} \text{ m}^2 \text{ V}^{-1} \text{ s}^{-1}$

Table I: Input parameters used for the simulations of the a-Si:H solar cell in the as-deposited state.

In order to simulate the quantum efficiency accurately, a multi-rough-interface optical model was used to calculate the e-h pair generation profile in the solar cell under an AM 1.5 spectrum. Light trapping effects were included also.

C. Degradation model

In our degradation model we describe the solar-cell performance degradation after high-energy electron irradiation by assuming that this degradation is the result of three effects: (i) the increase of the defect density, (ii) the increase of the activation energy of the doped layers, and (iii) the coloring of the glass. In order to model the first effect, the DCDP should scale with the non-ionizing energy deposition, the e-h pair generation rate or the appropriate recombination depth profile if the degradation is through displacements, ionization or recombination processes, respectively. We will now briefly describe how each of these effects is incorporated in the simulations.

In case of 1-MeV electrons, degradation through displacements or ionizing processes will both lead a uniform DCDP. Because the solar cell is thin compared to the stopping range of the incident particles, the ionizing and non-ionizing energy deposition is uniform across the solar cell. Therefore, to simulate degradation through displacements or ionizing processes, for each fluence and defect state (D_e , D_z , D_h), the DCDP is taken as:

$$\Delta D_{n,i}(d) = D_n, \quad (1)$$

where D_n is the appropriate increase in defect density.

To simulate degradation through recombination processes, for each irradiation fluence and defect state (D_e , D_z , D_h), the DCDP $\Delta D_{n,i}(d)$ is calculated using the as-deposited e-h recombination profile, $R_i(d)$, at open-circuit voltage conditions under electron-irradiation as follows:

$$\Delta D_{n,i}(d) = C_n R_i(d), \quad (2)$$

where d is the position in the device, n is a label for the defect type, and i a label indicating the i -layer thickness. The recombination profile, $R_i(d)$, is calculated using ASA when a uniform e-h pair generation profile is assumed. The generation-rate density is calculated using the IEL values as presented above. Note that the constants C_n are not dependent on the solar-cell thickness, but only on the fluence. C_h is taken negative, while C_e and C_z are taken positive in accordance to our charged deep-level transient spectroscopy (Q-DLTS) measurements [22]. To reduce the complexity of the model, we assume also that the constants are independent of the Fermi-level position, which is supported by Q-DLTS results reported by Zeman *et al.* [23] on light soaked a-Si:H in which an n-type or p-type DOS was programmed by bias annealing.

In this article the second effect (i.e., the increase of the activation energy of the doped layers) is accounted for by including changes in the dark-conductivity activation energy of the p- and n-layer. These changes are necessary to obtain good fits for the degradation of the open-circuit voltage (V_{oc}), as will be described below.

The third effect: the coloring of the glass was included in the optical simulations of the cells. Measured data of the change in transmission after irradiation was used as input parameter to describe the degradation of the TCO/glass substrates in the simulations.

To simulate the overall effect of the irradiation on the cells, the defect-creation depth profiles are added to the as-deposited defect-state distribution. The activation energies of the p and n-layer are changed in accordance to the measurement results. Using the new defect-state distribution, the new AM1.5 electron-hole generation profiles are calculated. The solar cell performance corresponding to the irradiated state is then determined and compared to the initial performance.

Other possible effects on the material as a result of the interaction with the electron beam were considered as well. However, no significant changes in the valence

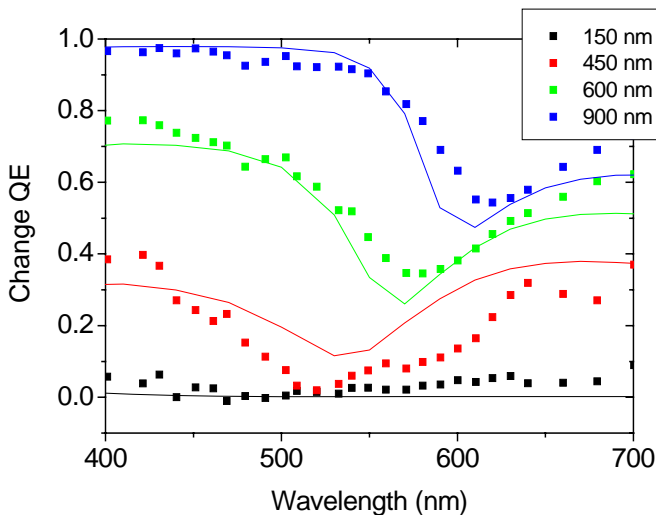


Figure 2: Measured (symbols) and simulated (lines) ΔQE for solar cells with a varying i-layer thickness after irradiation using a fluence of 1.9×10^{16} electrons/cm².

band tail after irradiation were observed by Danesh *et al.* [9] and in our dual-beam photoconductivity spectroscopy results. In addition, time-resolved microwave conductivity (TRMC) data suggest that the electron mobility does not change as a result of irradiation [13]. No changes in the bandgap of individual a-Si:H layers were found in RT measurements for the fluences used [22]. Therefore, all other model parameters have not been changed as a function of irradiation fluence.

IV. EXPERIMENT

Single junction a-Si:H solar cells were deposited on Asahi U-type substrates using plasma-enhanced chemical vapor deposition. The following structure was used: 10-nm p-type doped a-SiC:H layer, an i-layer with thickness ranging from 150 to 900 nm, and a 20-nm n-type a-Si:H layer. As back contact a stack of 200 nm silver and 100 nm aluminum was used. The deposition of the i-layer was carried out using a gas pressure of 0.7 mbar, a substrate temperature of 180°C, a power density of 150 W/m², and a silane gas flow of 40 sccm. The area of the solar cells was 0.1 cm². The solar-cell external parameters were obtained from *J-V* curves measured under AM1.5 illumination. The initial efficiency of the solar cells depends on the thickness of the intrinsic layer and rang from 5.5% to 8.5%. *QE* measurements were performed at zero bias and no bias light was used.

The solar cells were irradiated under open-circuit conditions using 1-MeV electrons. For the electron irradiation we employed a Van de Graaff accelerator, with a beam current density of 5×10^{11} electrons/cm²s;

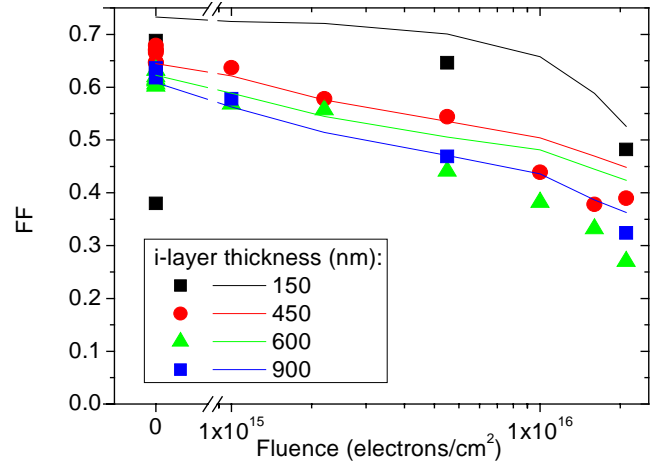


Figure 3: Measured (markers) and simulated (lines) FF as a function of the fluence for solar cells with a varying i-layer thickness.

the cells were irradiated with fluences ranging from 1×10^{15} electrons/cm² up to 1.9×10^{16} electrons/cm². A beam current of 5×10^{11} electrons/cm²s was used for fluences up to 1×10^{16} electrons/cm². Higher fluences were obtained using a current of 5×10^{11} electrons/cm²s for the first 1×10^{16} electrons/cm², and 1.5×10^{12} electrons/cm²s for the remaining irradiation fluence. Solar cells with an i-layer thickness of 450 or 600 nm were irradiated with 6 fluences, whereas for the other cells 3 fluences were used. Irradiation was performed at room temperature by placing the solar cells on a temperature-controlled table.

After irradiation the efficiencies of the solar cells dropped to approximately 1% to 3%. However, large part of this efficiency decrease can be ascribed to coloring of the glass substrates. If we correct for this coloring, the cell efficiencies are in between 1.5% and 7% (we used the *QE* data to estimate the short-circuit current of the solar cell). All cells were characterized within 3 days after irradiation in order to minimize annealing effects.

V. MATCHING SIMULATION RESULTS WITH EXPERIMENTS

Previously, experimental *QE* and *J-V* data results of solar cells with a varying i-layer thickness after 1-MeV electron irradiation have been matched with simulations using the degradation model to extract the DCDP [24,25]. A summary of the results is presented below.

Figure 2 shows the results for the change in *QE* (ΔQE) after an irradiation with a fluence of 1.9×10^{16} electrons/cm². This ΔQE is defined as

$$\Delta QE = (QE_{\text{initial}} - QE_{\text{irradiated}})/QE_{\text{initial}} \quad (2)$$

The thinner solar cells are least affected by the electron-beam irradiation. The 150-nm cell shows almost no change in QE, while the 900-nm cell degraded more than 40% across the investigated wavelength range and almost completely for wavelengths below 500 nm. A minimum in ΔQE is typically found for wavelengths between 500 to 625 nm. The minimum in ΔQE seems to shift to longer wavelengths for thicker solar cells. For lower irradiation fluence similar effects were observed as in Figure 2, but the effects were less pronounced. Figure 2 also shows the corresponding simulated ΔQE results (lines). In the simulations we assumed that the DCDP is linked to the total recombination profile. By matching the simulations to the measurement results the following values for C_e , C_z , and C_h were obtained: 3.4×10^{-3} s, 2.0×10^{-2} s, and -2.0×10^{-5} s, respectively. With these values the ΔQE for each thickness is generated in one simulation run. Overall a good fit could be obtained between simulation and experiment, i.e., the observed trends found in the measured data are also obtained in the simulated results. The difference between the measured and simulated ΔQE is typically within 0.1. However, some discrepancies can be seen as well, mainly for long wavelengths and for the 450-nm cell.

The fill factor (FF) is typically seen as a good indication for the total recombination in the cell. The experimental results (markers) for the FF are given in Figure 3. As-deposited fill factors were in between 0.6 and 0.7, depending on the thickness. After degradation, FF dropped to values between 0.16 and 0.31. The thickness dependence of the FF is obscured due to the variation in quality of the initial cells, but it seems that thinner cells show higher as-deposited FF s and less degradation.

The simulation results (see Figure 3, lines) show similar trends, and overall a good match is obtained. As-deposited simulated FF s were between 0.6 and 0.73, with the thinner solar cells having a higher FF . After degradation FF dropped between 0.20 and 0.25. Note that the 150-nm cell does show a great radiation tolerance up to 1×10^{16} electrons/cm². Again, at higher fluence the simulations tend to underestimate the degradation.

Overall, the degradation model provides reasonable to good matches with the experimental data of 1-MeV electron irradiated a-Si:H solar cells.

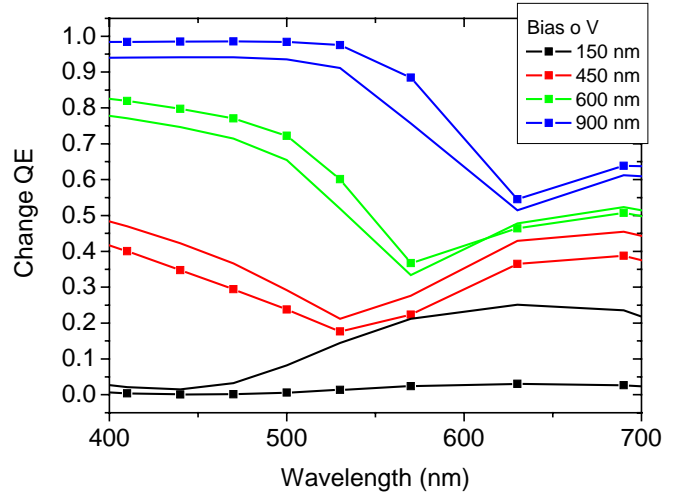


Figure 4: Simulations of the change in QE for solar cells with a varying i-layer thickness when the DCDP is taken uniform (lines) and when it is profiled using the recombination rate (lines + markers).

VI. SIMULATION ASSUMPTIONS

In the previous section we presented a match between experimental results and simulations, assuming that the defect increase was due to recombination events via defect states. In order to verify the validity of this approach, we studied the influence of three assumptions in our simulation model for the degradation: (A) The shape of the DCDP: uniform or linked to the recombination profile, (B) the type of recombination profile: valence-band tail recombination versus total recombination (i.e., including recombination via defect states), and (C) the effect of the activation energy of the doped layers.

To visualize the influence of the above assumption in our simulations we show the results for degradation by 1.9×10^{16} electrons/cm². At this fluence effect of the i-layer thickness, and thus the DCDP on the degradation is most apparent.

A. Defect creation depth profile

If the induced damage by the electron beam is associated with displacements or ionizing processes, a uniform and equal defect-creation depth profile is expected for each solar cell thickness (case 1, Equation 1). If the degradation is due to recombination processes, the defect-creation depth profile is similar in shape as the recombination depth profile (case 2, Equation 2). Figure 4 shows simulations of the change in QE for solar cells with a varying i-layer thickness when the DCDP are taken uniform (lines) and when it is profiled using the

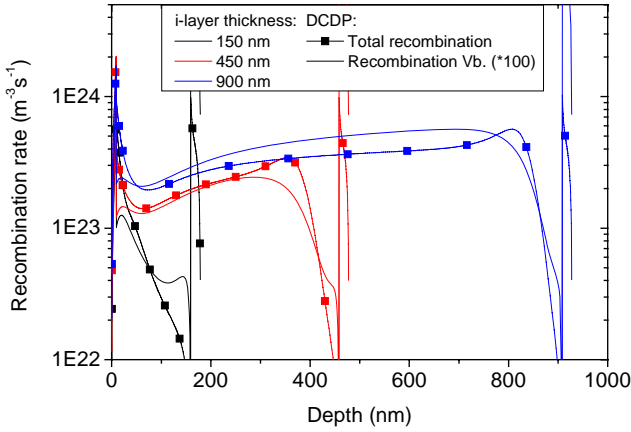


Figure 5: Recombination profiles for the recombination through the valence band tail (lines) and the total recombination (lines + markers) for the 150-nm, 450-nm and 900-nm cell. Here, the recombination through valence band tail states is multiplied by 100.

recombination rate (lines + markers). For the first case the defect density of the D_e , D_z , and D_h were increased by 1.7×10^{17} , 6.8×10^{17} , and -3.8×10^{15} defects/cm³, respectively. For the second case, the multiplication C_e , C_z , and C_h factors were chosen as 0.685 s, 2.80 s, and 0.016 s, respectively. (Note, compared to the simulations in presented section V, a lower electron-hole generation rate was used, which corresponds better with the expected values based on IEL calculations. However, equal amount of defects is created in both cases.) In both cases the same ratios for the changes in defect density for the 3 defect states are used.

The shape of the ΔQE graphs is not affected significantly by the choice of DCDP, even though the defects are created at different positions in the cell. In case of a uniform defect-creation profile, more defects are generated near the p-i interface as compared to the DCDP calculated from the recombination rate density. For both DCDPs a minimum in ΔQE is observed between 450 and 650 nm and this minimum shifts toward higher wavelength when increasing the i-layer thickness. However, the main difference between both cases is in the influence of the i-layer thickness on the degradation. This thickness influence is more pronounced in case the DCDP is profiled with the recombination rate density. For the 150-nm cell a uniform DCDP results in more degradation, and for the 900-nm cell less.

The external parameters show a similar trend. The difference in FF between the 150 and 900-nm cell after degradation is in case of a uniform DCDP 0.077 and for the recombination case 0.170. (For V_{oc} the difference is

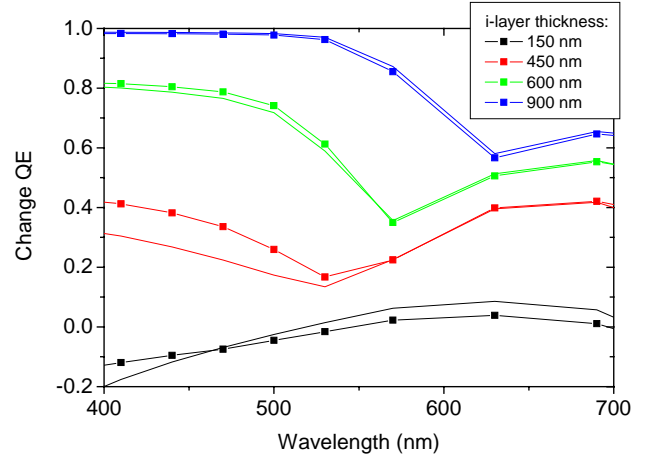


Figure 6: ΔQE when DCDP is calculated using valence band tail recombination (lines) or total recombination (lines + markers).

3.2 mV vs. 4.6 mV, for J_{sc} this is 23.8 vs. 8.9 A/m², and for the efficiency this is 1.22 % vs. 0.45 %). From these simulations it is concluded that a better match is obtained with the experimental data as presented in section V if the DCDP is profiled with the recombination rate.

The larger difference in degradation between the 150 and 900 nm cell range for the second case is explained as follows. The thicker as-deposited solar cells have a higher recombination rate density in the bulk of the i-layer. Thus according to the model the defect density in the thicker solar cells is increased more as compared to the thinner solar cells leading to a larger difference in the performance after irradiation for each i-layer thickness.

B. Valence band tail recombination versus defect recombination

In our degradation model we have linked the DCDP to the recombination profile. However, it is often proposed that Staebler-Wronski degradation is related to the creation of defects by electron-hole recombination events on weak-bonds [26]. Then the recombination through the valence band tail is the governing factor in the degradation. Two different recombination depth profiles in our degradation model are tested and compared with each other: the total recombination (case B.1) and the recombination through valence band tail states (case B.2).

Figure 5 shows both recombination profiles for the 150, 450 and 900-nm thick solar cells. All profiles have approximately the same shape. For both cases there is a large peak in the recombination rate in the p- an n-layer, due to the high defect density in those layers. For the thicker solar cells, there is a low recombination rate

density near the p-i interface and it increases through the bulk towards the i-n interface. At the i-n interface there is another drop in recombination rate density. The 150-nm cell shows a decreasing recombination rate density throughout the i-layer. The recombination through the valence band tail states is between one and two orders lower and shows a ‘flatter’ recombination profile in the bulk, and does not exhibit a peak in recombination rate density before the drop near the i-n interface.

In the degradation model we used the following parameters for the simulations using the total recombination: $C_e = 0.685$ s, $C_z = 2.80$ s and $C_h = 0.016$ s. If recombination through the valence band tail is assumed C_e , C_z , and C_h were taken as 61.2 s, 250.3 s and 1.4 s, so that the QE results for both profiles show a similar amount of degradation. The ratios between C_z , C_h , and C_e are left unchanged. The activation energy of both doped layers is increased by 0.15 eV. The resulting ΔQE curves for both recombination profiles are shown in Figure 6. For the 600 and 900-nm cells no differences between both procedures are observed. For the thinner solar cells, the difference is only significant for wavelengths below 550 nm. Profiling the DCDP with the recombination rate through the valence band tail, will then lead to a lower degradation in QE .

Exchanging the total recombination profile with the recombination through valence band tail states profile in the degradation model, will lead to a increase up to 1% in V_{oc} , while lowering the FF between 4% and 10%. The J_{sc} decreases up to 4%. The thinner cells show the most change in FF , while the thicker cells exhibit most change in J_{sc} .

C. Activation energy versus the V_{oc}

In our degradation model changes in the activation energy of the doped layers are included. These changes have been observed after irradiating n-doped and p-doped 500-nm thick layers. In these measurements a change of 0.2 to 0.25 eV after a fluence of 19×10^{15} 1-MeV electrons/cm² was observed.

Figure 7 shows the change in QE when the changes in dark activation energy of the doped layers are (not) included. A change of 0.15 eV was used in the simulations. The changes in the defect density between both simulations are unchanged. The multiplication factors C_e , C_z , C_h were taken to be 0.685 s, 2.8 s, and 0.0116 s, respectively. Overall, increasing the activation energy will lower the QE , except for the 150-nm cell. For that cell the QE below 550 nm was increased. The

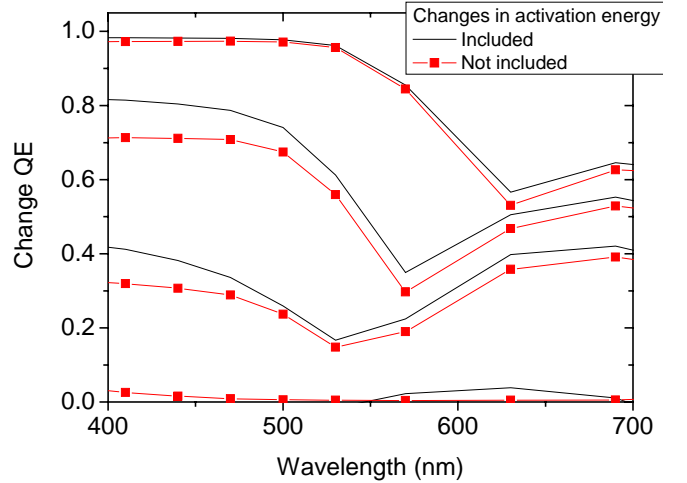


Figure 7: Change in electrical QE using the same multiplication parameters, but with (lines) and without (lines and markers) changes in the dark activation energy of the doped layers included.

ΔQE shows a maximum change of 0.1, primarily at lower wavelengths. In addition, the ΔQE will show less of a plateau at the lower wavelengths, resembling more the obtained experimental results.

Changes in the activation energy instead of in the defect density have also a different effect on the external parameters. The change in defect density leads to a decrease of 4%, 21%, and 10% in, respectively, the V_{oc} , J_{sc} , and FF . Changing the activation energy in addition to the defect density will lead to an extra 10%, 7%, and 7% change in the external parameters. Including changes in the activation energy of the doped layer is a necessary method to obtain good match with the experimental results for the V_{oc} , while also maintaining good matches for the FF and especially for J_{sc} . In addition, it improves the match with the experimental QE for wavelengths below 500 nm

VII. CONCLUSIONS

In the literature the defect creation mechanism of high-energy charged particle irradiation of a-Si:H solar cells is debated. We presented an alternative method to deduct the defect mechanism by irradiating a-Si:H solar cell with a varying i-layer thickness and then matching the results with computer simulations. In the simulations we describe the degradation to three effects: changes in the defect density of the material, changes in the dark activation energy of the doped layers, and to the coloring of the glass. With the model a good match is obtained with experimental results of the performance

degradation of the irradiated solar cells for each i-layer thickness.

The simulations provide a good match with the experimental results for each solar cell thickness if the DCDP is correlated to the recombination processes in contrast to a uniform DCDP. Profiling the changes in the defect density of states using the recombination rate on weak bonds does further improve the match between simulations and experiments. This indicates a strong link between high-energy electron irradiation and the Staebler-Wronski effect.

Finally, changing the activation energy of the doped layers was essential in obtaining good matches for the V_{oc} after degradation; while the match for other parameters, especially the J_{sc} and QE , which also did show small improvements.

VIII. ACKNOWLEDGEMENTS

This work is supported by STW, Novem, and Dutch Space. The authors thank Martijn Tijssen, Arjan Driessen, and Marinus Hom for their technical assistance.

REFERENCES

-
- [1] Navid S. Fatemi, Howard E. Pollard, Hong Q. Hou, Paul R Sharps, in: *Proceedings of the 28th IEEE Photovoltaic Specialists Conference 2000*, 1083 (2000).
- [2] R. C. Alig, S. Bloom, C. W. Struck, *Phys. Rev. B*, **22** (12), 5565 (1990).
- [3] M. J. Berger, J. S. Coursey, M. A. Zucker, *ESTAR database*, <http://physics.nist.gov/PhysRefData/Star/Text/>
- [4] G. P. Summers, E. A. Burke, P. Shapiro, S. R. Messenger, R. J. Walters, *IEEE Trans. Nuclear Science* **40** (6), 1372 (1993).
- [5] Q. Wang, K. Lord, J. R. Woodyard, *Conference Record of the 28th IEEE Photovoltaic Specialists Conference 2000*, 1057 (2000).
- [6] G. J. Vendura, M. A. Kruer, R. M. Kurland, J. Newton, *Conference records of the first WCPEC*, 2049 (1994).
- [7] J. R. Srour, G. J. Vendura, D. H. Lo, C. M. C. Toporow, M. Dooley, R. P. Nakano, and E. E. King, *IEEE Trans. Nucl. Sci.*, **45**, 2624 (1998).
- [8] R. J. Walters, J. H. Warner, G. P. Summers, S. R. Messenger, J. R. Lorentzen, P. Tlomak, J. E. Granata, P. E. Hausgen, *19th European Photovoltaic solar cell conference*, 3606 (2004).
- [9] P. Danesh, B. Pantchev, I. Savatinova, E. Liarokapis, S. Kaschieva, A. G. Belov, *Vacuum*, **69**, 79 (2003).
- [10] D. L. Staebler, C. R. Wronski, *Appl. Phys. Lett.*, **31**, 292 (1977).
- [11] M. Cutrera, R.R. Koropecski, A. M. Gennaro, R. Arce, *Phys. Rev. B*, **35**(3), 1442 (1987).
- [12] N. Kishimoto, H. Amekura, K. Kono, C.G. Lee, *J. Non-Cryst. Solids*, **227-230**, 238 (1998).
- [13] A. Klaver, J. M. Warman, M. P. de Haas, J. W. Metselaar, R.A. C. M. M. van Swaaij, *Mat. Res. Soc. Symp. Proc.* **808**, 165 (2004).
- [14] F. Diehl, W. Herbst, S. Bauer, B. Schroeder, H. Oechsner, *J. Non-Cryst. Solids* **198-200**, 436 (1996).
- [15] M. Zeman, J. A. Willemen, L. L. A. Vosteen, G. Tao, J. W. Metselaar, *Solar Energy Mater. Solar Cells*, **46**, 81 (1997).
- [16] M. Zeman, R. A. C. M. M. Van-Swaaij, E. Schrotten, L. L. A. Vosteen, J. W. Metselaar, *Mat. Res. Soc. Symp. Proc.* **507**, 409 (1999).
- [17] B. E. Pieters, J. W. Metselaar, M. Zeman, in: *Conference Record of the 20th European Photovoltaic Solar Energy Conference and Exhibition* (2005).
- [18] M. Zeman, J. A. Willemen, L. L. A. Vosteen, G. Tao, J. W. Metselaar, *Solar Energy Materials and Solar Cells*. **46**(2), 81 (1997).
- [19] M. A. Kroon, R. A. C. M. M. van Swaaij, M. Zeman, V. I. Kuznetsov, J. W. Metselaar, *Appl. Phys. Lett.* **72**(2), 209 (1998).
- [20] M. Zeman, V. Nadazdy, J. W. Metselaar, *Mat. Res. Soc. Symp. Proc.* **808**, 189 (2004).
- [21] M. J. Powell, S. C. Deane, *Phys. Rev. B.*, **53**, 10121 (1996).
- [22] A. Klaver, unpublished results.
- [23] M. Zeman, V. Nadazdy, R. Durny, J. W. Metselaar, to be published in MRS proceedings 2005.
- [24] A. Klaver, J.W. Metselaar, M. Zeman, R. A. C. M. M. van Swaaij, in: *Proceedings of the 31st IEEE Photovoltaic Specialists Conference 2005*, 1440 (2005).
- [25] A. Klaver, J. W. Metselaar, M. Zeman, R. A. C. M. M. van Swaaij, in: *Conference Record of the 20th European Photovoltaic Solar Energy Conference and Exhibition*, (2005).
- [26] R. A. Street, *Physica B*, **170**, 69 (1991).